2014 IEEE International Conference on Robotics & Automation (ICRA)
Hong Kong Convention and Exhibition Center
May 31 - June 7, 2014. Hong Kong, China

Power-continuous Synchronisation of Oscillators: a novel, energy-free way to synchronise dynamical systems

Gerrit A. Folkertsma
Robotics and Mechatronics group
CTIT institute
University of Twente
g.a.folkertsma@ieee.org

Arjan J. van der Schaft
Johann Bernoulli Institute for
Mathematics and Computer Science
University of Groningen
a.j.van.der.schaft@rug.nl

Stefano Stramigioli
Robotics and Mechatronics group
CTIT institute
University of Twente
s.stramigioli@ieee.org

***Abstract*— Synchronisation is an essential part of many controlled dynamical systems, in particular in the limb motion of legged robots. In this paper we introduce a novel control strategy that allows synchronisation of two oscillators without using any external power, but by modulating the power flow between the two oscillators. We then derive a separate energy-level controller that regulates the oscillation amplitude, again without changing the system's total energy. Finally, we show that the strategy works on a realistic mechanical system, by synchronising the phase difference and apex height of two bouncing masses.**

I. Introduction

From chaotic oscillators to second-order dynamic systems, many control problems for physical systems require some form of synchronisation of various parts of the system. Think of footfall patterns in locomotion, determined by the relative phase of leg movement; periodically firing neural networks; or even voltage converters on a three-phase power grid [1]. For the field of robotics—and specifically that of legged locomotion—the synchronisation of limb movement is of key importance.

Control theory has learned from biology by using Central Pattern Generators (CPGs) to generate trajectories or motion profiles that are synchronised between various body parts [2]–[4]. However, for high-speed, energy-efficient dynamic locomotion, some research is moving towards resonance-based locomotion—a form of morphological computation—for which CPGs might not be the best solution [5], [6]. Indeed, it would be beneficial to directly synchronise the actual system oscillation, rather than the setpoint generators.

The Kuramoto model is widely used for the study of large networks of phase oscillators, but is less suited to the study of mechanical oscillators [7], [8]. Other work has already been done on mechanical oscillator synchronisation, but usually synchronisation is achieved by coupling through dampers, or by external actuators [9], [10]. While the damper-coupling method is a physically intuitive way of synchronisation that fits the morphological computation framework, neither method preserves the system's energy.

In this paper we present a physically intuitive way to achieve phase synchronisation of physical oscillators: by influencing the oscillation frequency of one of the oscillators, it is possible to make it "move ahead of" or "lag behind" the other oscillator: thus the phase difference can be controlled. This idea is similar the Adaptive Frequency Oscillators of Buchli et al [11], in the sense that the oscillator's *intrinsic* frequency is changed. Our method is different in that our oscillator is the actual physical system, rather than the setpoint generator. Most importantly, we will achieve the synchronisation in a completely passive way, i.e. *without using any energy*.

We influence the oscillation frequency by changing the spring stiffness of a mass-spring system in a physically consistent way. Using Port-Hamiltonian systems theory we prove that we indeed neither supply nor extract energy from the system. Because of the bondgraph representation, the method is very general (not domain specific) but also abstract. At the end of this paper we look briefly at the application of the method to a realistic mechanical system.

II. Synchronisation

We start with a simple oscillating system, for which we can easily find the system equations. We prove that the system is power-continuous, i.e. passive, and show that we can synchronise the phase of the two sub-systems.

A. System

The system consists of two mass-spring systems in which the spring stiffness can be modified by the controller: see Fig. 1. Changing a spring's stiffness takes effort unless the spring is unloaded, so the proper way to model a spring with variable stiffness is by a two-port **C**-element. The one port is the usual mechanical port with the conjugate power pair $(e, f) = (F, \dot{x})$; the other is the stiffness-changing port with conjugate power pair $(e, f) = (e_K, \dot{K})$. The constitutive relations for these ports are readily found from the spring's energy function $H(x, K)$ (1); from (3) it is clear that changing the stiffness is indeed associated with an effort if $x \neq 0$.

$$H(x, K) = \frac{1}{2} K x^2 \tag{1}$$

$$F = \frac{\partial H(x, K)}{\partial x} = Kx \tag{2}$$

$$e_K = \frac{\partial H(x, K)}{\partial K} = \frac{1}{2} x^2 \tag{3}$$

978-1-4799-3684-7/14/$31.00 ©2014 IEEE

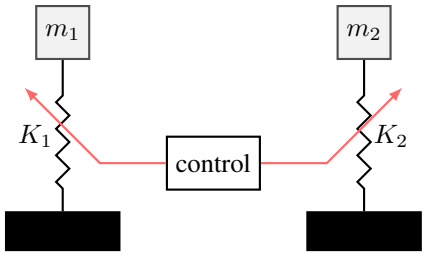

Fig. 1: Double mass-spring system, with a controller to modify the spring stiffness.

The advantage in the case of synchronisation is that we will always be influencing the two springs in opposite ways: if one oscillator must move ahead in phase and the other backwards, the one spring stiffness must increase whilst the other must decrease. $\dot{K}_1$ and $\dot{K}_2$ will therefore have opposite signs and, since $e_K = \frac{1}{2}x^2$ is always positive, the power required for increasing the first spring's stiffness can be extracted from the other.

The bondgraph model in Fig. 2 shows that this "power pumping" from one spring to the other is directly realised by connecting the stiffness ports of the springs by a (modulated) gyrator. This two-port non-storage element gyrates as (4), changing effort to flow with ratio r.

$$\begin{pmatrix} f_2 \\ f_1 \end{pmatrix} = r \cdot \begin{pmatrix} e_1 \\ e_2 \end{pmatrix} \tag{4}$$

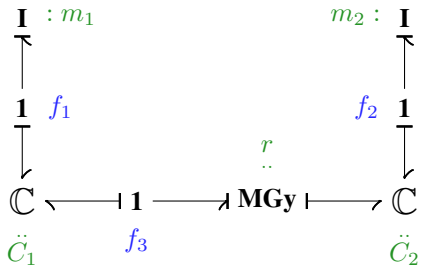

Fig. 2: Bondgraph model of the double mass-spring system.

Since the physical part of the system is now complete, we first derive the complete Port-Hamiltonian system equations (5) to show that the system is indeed fully passive. The Hamiltonian in (6) consists of four terms, one for each storage element.

$$\dot{\boldsymbol{x}} = (J(\boldsymbol{x}) - R(\boldsymbol{x})) \cdot \nabla \mathcal{H}(\boldsymbol{x}) \tag{5}$$

$$\mathcal{H}(\boldsymbol{x}) = \frac{p_1^2}{2m_1} + \frac{1}{2}K_1 x_1^2 + \frac{1}{2}K_2 x_2^2 + \frac{p_2^2}{2m_2} \tag{6}$$

The state vector $\boldsymbol{x}$ contains the position (x_i) and momentum (p_i) of the two masses, and the stiffnesses of the springs (K_i). There is no damping in the system, so $R(\boldsymbol{x}) \equiv 0$. The interconnection matrix $J(\boldsymbol{x})$ is found by inspection of Fig. 2 and given in (7). From the skew-symmetry of $J(\boldsymbol{x})$ follows that it is a proper Dirac structure and the system is indeed power-continuous, with $\mathcal{H}(\boldsymbol{x})$ a conserved quantity [12].

Note that $J(\boldsymbol{x}) = J$ does not depend on the system state, but only on the gyration ratio r. Because this is a modulation and not a power port, we can freely—that is, without power cost—control it to influence the system behaviour.

$$\begin{pmatrix} \dot{x}_1 \\ \dot{p}_1 \\ \dot{K}_1 \\ \dot{x}_2 \\ \dot{p}_2 \\ \dot{K}_2 \end{pmatrix} = \begin{bmatrix} 0 & 1 & 0 & 0 & 0 & 0 \\ -1 & 0 & 0 & 0 & 0 & 0 \\ 0 & 0 & 0 & 0 & 0 & r \\ 0 & 0 & 0 & 0 & 1 & 0 \\ 0 & 0 & 0 & -1 & 0 & 0 \\ 0 & 0 & -r & 0 & 0 & 0 \end{bmatrix} \cdot \begin{pmatrix} K_1 x_1 \\ p_1/m_1 \\ x_1^2/2 \\ K_2 x_2 \\ p_2/m_2 \\ x_2^2/2 \end{pmatrix} \tag{7}$$

B. Experiment

1) Controller: To control the phase difference between the two subsystems, we need a measure for the phase. There are many options, the choice of which depends on the application. In this simple model, we look at the (x, v) phase portrait of the two masses and use the angle of a vector pointing from the origin to the point representing the current state as a phase angle, calculated by the four quadrant arctangent of (v/x) (8). We define the phase difference as $\theta := \phi_2 - \phi_1$.

$$\phi_i := \text{atan2}(v_i\ ,\ x_i) \in [0, 2\pi), \quad i \in \{1, 2\} \tag{8}$$

Since the modulated gyrator automatically takes care of the power flow between the springs, a simple PID controller on the phase difference error with respect to setpoint θ_s, calculating the gyration ratio r, suffices for control (9). Fig. 3 shows the complete system.

$$r = K_P \cdot \left(1 + \frac{1}{\tau_i s} + \tau_d s\right) \cdot (\theta - \theta_s) \tag{9}$$

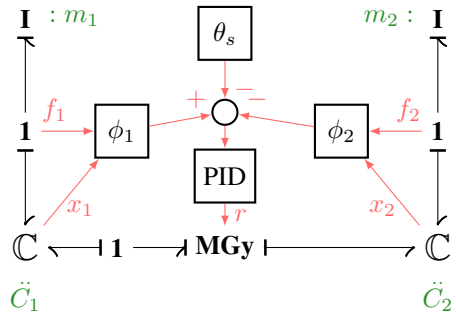

Fig. 3: Bondgraph model of the double mass-spring system with synchronisation controller.

2) Simulation: Using a simulation package that can directly simulate bondgraph models [13], we validate the system by initialising the oscillators such that they start in phase ($\theta = 0$) and then changing the phase setpoint according to (10). All parameters as used in the simulation can be found in Table I and the initial configuration is given in (11).

$$\theta_s = \begin{cases} 0 & t < 10 \\ \frac{t-10}{20}\pi & 10 \le t < 30 \\ \pi & t \le 30 \end{cases} \tag{10}$$

TABLE I: Parameters as used in the simulation.

m_1	m_2	K_P	τ_i	τ_d
0.8 kg	1 kg	0.2	10 s	15 s

$$\begin{pmatrix} x_1 \\ p_1 \\ K_1 \\ x_2 \\ p_2 \\ K_2 \end{pmatrix} |_{t=0} = \begin{pmatrix} 0\,\mathrm{m} \\ 1\,\mathrm{kg\,m\,s^{-1}} \\ 1\,\mathrm{N\,m^{-1}} \\ 0\,\mathrm{m} \\ 1\,\mathrm{kg\,m\,s^{-1}} \\ 1\,\mathrm{N\,m^{-1}} \end{pmatrix} \tag{11}$$

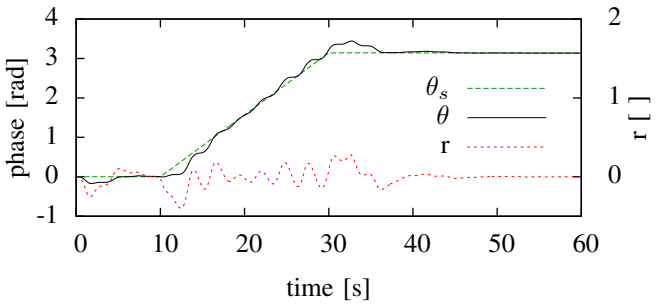

Fig. 4: Phase difference and control signal of the system during the synchronisation experiment.

The simulation results in Fig. 4 show that the phase difference θ neatly follows the setpoint. The changing phase difference is also clear from Fig. 5, where the stiffness plot shows that K_2 is increased to cause it to move forward in phase w.r.t. subsystem 1, then decreased again to settle. Notice that towards the end, when θ_s is constant, spring 2 automatically retains a higher stiffness than spring 1, because of the higher mass m_2.

From the amplitudes of x_1 and x_2, but especially from the energy levels in Fig. 6, the exchange of power between the two oscillators through the modulated gyrator is evident. At first, power flows to subsystem 2 to match the oscillation frequencies and keep $\theta = 0$; then even more power is allowed to flow from 1 to 2, facilitating the phase difference increase. Next, subsystem 2 is slowed down by letting power flow back to subsystem 1 and finally in steady state r returns to 0 (Fig. 4) and no more power is exchanged between the springs.

The most important result is the combination of Figs. 4 and 6: we have achieved phase synchronisation (with arbitrary phase difference) in a completely power-continuous, i.e. passive, way.

III. Energy control

Although we did achieve phase synchronisation with the system in Fig. 3, there is one side effect of the control method: because power is transferred between the two oscillators, their energy levels change and as a result, at the

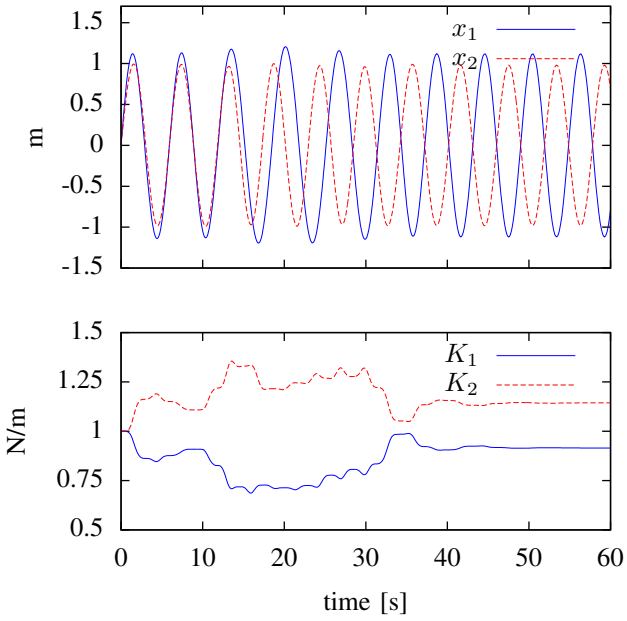

Fig. 5: Mass position and spring stiffness during the synchronisation experiment.

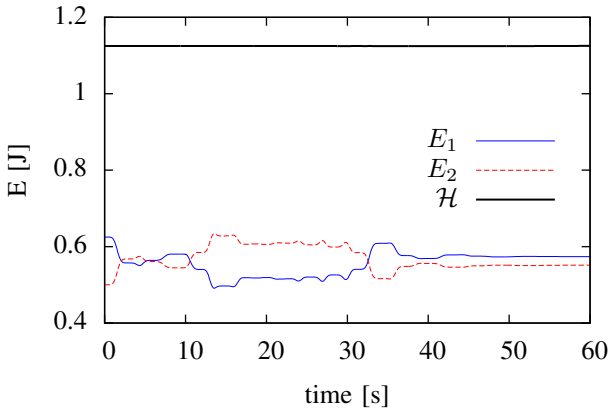

Fig. 6: Energy levels during the synchronisation experiment: the sum of kinetic and potential energy of subsystem 1, subsystem 2 and the total system energy $\mathcal{H}$.

end of the simulation the amplitudes of the two oscillators have changed (see Fig. 5 after $t = 40\,\mathrm{s}$). This might be undesirable, for instance if the system does not simply consist of two oscillators, but of two "bouncing" parts of a bounding quadruped. Therefore, in this section we present a way to also control the amplitude of the two oscillators—again, in a power-continuous way.

A. Energy level controller

To stay close to the power-based modelling, we derive an energy level controller that aims to keep the total energy in a subsystem constant at a desired level. First, the desired

energy is calculated from the desired amplitude x_s (12). The actual energy is most easily determined whenever the spring's deflection is at its maximum, i.e. when v crosses 0 from above (13).

To inject energy into the system, an estimate is made for the duration of the next oscillation period, so the amount of power to be injected during that time, P_C, can be calculated. In the case of an oscillator, the period estimate follows from the current stiffness and the mass (14); in the case of a "bouncing" robot leg this would be the stride time, or ground contact time.

$$E_s = \frac{1}{2} K x_s^2 \tag{12}$$

$$E = \frac{1}{2} K (x|_{v\downarrow=0})^2 \tag{13}$$

$$T = 2\pi / \sqrt{\frac{K}{M}} \tag{14}$$

$$P_C = -(E - E_s)/T \tag{15}$$

The power is applied to the mass through a force actuator: since $P = \langle e, f \rangle = F^\top v$, the required actuator force can be calculated by (16)—taking care that F does not become infinite when $v \approx 0$—where v is the speed of the mass, $\dot{x}$.

$$F = \begin{cases} 0 & v = 0 \\ \text{limit}(\frac{P_C}{v}, -0.2, 0.2) & v \neq 0 \end{cases} \tag{16}$$

B. Augmented model

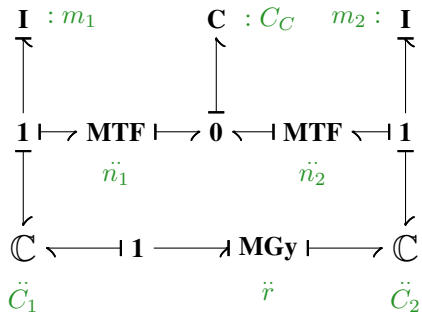

Fig. 7: Bondgraph model of the double mass-spring system with energy control: an extra storage element acting as a buffer allows two modulating transformers to inject or extract power from the two oscillators.

In order to keep the total system power continuous, instead of adding plain force actuators we augment the system as shown in Fig. 7. One extra **C**-type storage element has been added as a buffer, connected to the two oscillators through modulated transformers. These two **MTF**-elements introduce two new control inputs to provide the required force from (16) to the subsystems.

From the constitutive equation of a modulated transformer (17) it is easy to find n such that e_1, the force applied to the mass, equals F (18):

$$\begin{pmatrix} e_1 \\ f_2 \end{pmatrix} = n \begin{pmatrix} e_2 \\ f_1 \end{pmatrix} \tag{17}$$

$$n = \begin{cases} \frac{F}{e_2} & e_2 \neq 0 \\ 0 & e_2 = 0 \end{cases} \tag{18}$$

The Port-Hamiltonian System equations of Fig. 7 are now augmented with an extra state (x_c of the buffer) and the three modulating control inputs r, n_1 and n_2 now appear in the interconnection matrix. This matrix is still skew-symmetric, so we still have a power-continuous system.

$$\mathcal{H}(\boldsymbol{x}) = \frac{p_1^2}{2m_1} + \frac{K_1}{2} x_1^2 + \frac{K_2}{2} x_2^2 + \frac{p_2^2}{2m_2} + \frac{K_C}{2} x_C^2 \tag{19}$$

$$\dot{\boldsymbol{x}} = \begin{bmatrix} 0 & 1 & 0 & 0 & 0 & 0 & 0 \\ -1 & 0 & 0 & 0 & 0 & 0 & -n_1 \\ 0 & 0 & 0 & 0 & 0 & r & 0 \\ 0 & 0 & 0 & 0 & 1 & 0 & 0 \\ 0 & 0 & 0 & -1 & 0 & 0 & -n_2 \\ 0 & 0 & -r & 0 & 0 & 0 & 0 \\ 0 & n_1 & 0 & 0 & n_2 & 0 & 0 \end{bmatrix} \nabla \mathcal{H}(\boldsymbol{x}) \tag{20}$$

C. Simulation

The model in Fig. 7 is simulated with the same phase difference controller as the one shown in Fig. 3, but with the addition of the control laws described in equations (12) – (18). The initial conditions are given in (21) and parameters are as listed in Table I, with $K_C = 100\,\mathrm{N\,m^{-1}}$. θ_s is the same as in the other experiment (10), but additionally the amplitude setpoint for oscillator 1 changes from 1 m to 2 m at $t = 60$ s.

$$\begin{pmatrix} x_1 \\ p_1 \\ K_1 \\ x_2 \\ p_2 \\ K_2 \\ x_C \end{pmatrix} |_{t=0} = \begin{pmatrix} 1.4\,\mathrm{m} \\ 0\,\mathrm{kg\,m\,s^{-1}} \\ 1\,\mathrm{N\,m^{-1}} \\ 0.5\,\mathrm{m} \\ 0\,\mathrm{kg\,m\,s^{-1}} \\ 1\,\mathrm{N\,m^{-1}} \\ 0.18\,\mathrm{m} \end{pmatrix} \tag{21}$$

Firstly, the simulation results in Fig. 8a show that the phase controller is still functional, even though shortly after $t = 60$ s it has to reject a disturbance caused by the energy injection from the other controller. Fig. 8b shows that the amplitude controller is also working, initially steering both oscillators to 1 m and then the first up to 2 m.

The energy levels in the energy level controller are shown in Fig. 9a. These are sampled once each oscillation period, when x is maximum. Although the phase controller changes the energy of each oscillator, as was also seen in Fig. 6, the energy level controller is able to reject this disturbance.[1]

Finally, Fig. 9b shows the actual energy levels in the two subsystems, in the coupling buffer, and the total system

[1]Because F has been limited as per (16), it actually takes 2 periods to increase the energy of the first oscillator to the new setpoint.

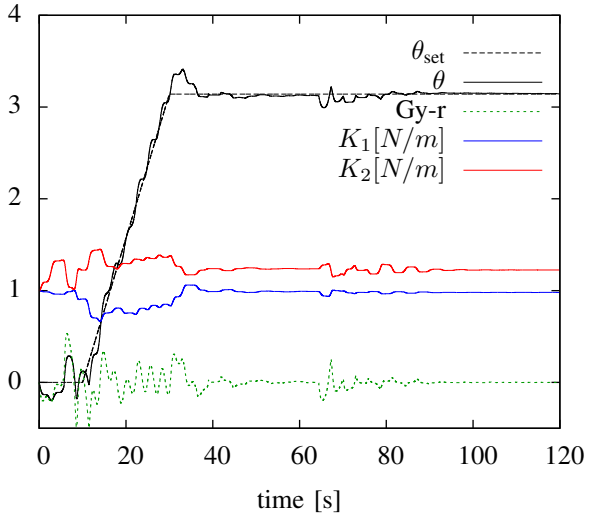

(a) Phase difference, gyration ratio and spring stiffness during the energy controller experiment. Note that after $t = 60\,\mathrm{s}$ the phase difference is disturbed by the energy controller pumping energy into subsystem 1, but the gyrator quickly stabilises.

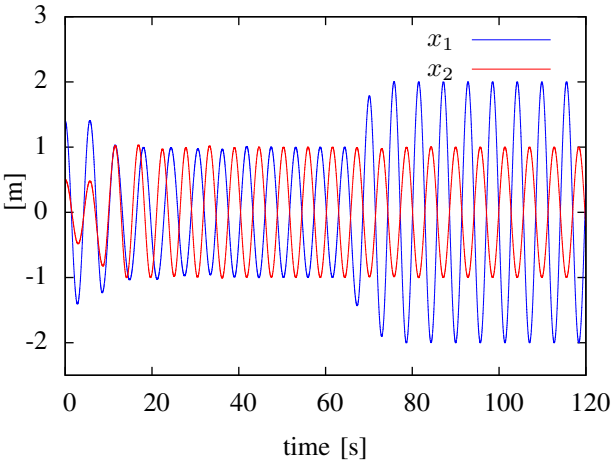

(b) Mass positions, showing first regulation towards an amplitude of 1 m, then an increase for subsystem 1 while maintaining the desired phase difference.

Fig. 8: Phase difference control during the synchronisation and energy level control experiment.

energy. During the first few seconds, when one oscillator's amplitude is too high and the other's too low, energy flows through the buffer from subsystem $1 \rightarrow 2$ and the buffer's net energy level change is 0. Later, when the first oscillator's amplitude is increased, the buffer's energy is transferred to the oscillator.

Of course, one might argue that calling the system passive while using energy from a buffer in the system is "cheating". However, as mentioned the net energy level change in the buffer up to $t = 60\,\mathrm{s}$ is zero; only when increasing the amplitude of the first oscillator—which simply requires more energy than was present in the two oscillators combined—do we use the contents of the buffer.

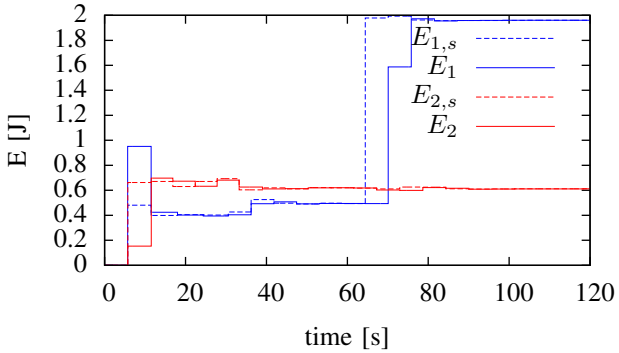

(a) Energy controller levels: sampled at every period, when x is at its maximum. Note that the energy level setpoints change, even though the amplitude setpoint is constant, due to a changing K caused by the phase controller.

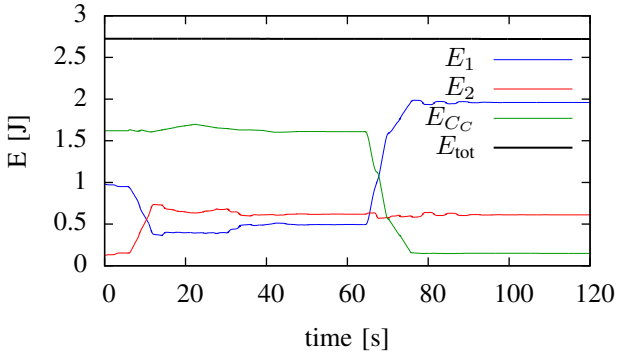

(b) System energy levels: firstly the amplitudes of the two oscillators are regulated towards 1 m, with the coupling spring only acting as a buffer; later increasing the first oscillator's amplitude thus energy by using up the buffer's energy. The total system energy is constant.

Fig. 9: Energy levels during the synchronisation and energy level control experiment.

IV. Hybrid Dynamics: Hopping Robot

To make the results more tangible, we have applied the control methods of the previous two sections to a hopping robot that consists of a body, a springy leg and a foot. The two-port C-element is replaced by a variable stiffness actuator. Two of these combined could form a "bipedal quadruped", able to bound and pronk in the sagittal plane. Currently, they can still only hop on the spot (Fig. 10). The energy level controller aims for an apex height of 1 m, while the phase difference is regulated towards 90°.

The control problem here is more challenging, because energy can only be injected during stance and stiffness modulation of the spring will only influence the ground phase. As such, both the energy level and phase difference controller have become discrete, updating only once every bounce or "stride". Due to this intermittent and limited control window, it does take a number of strides to achieve synchronisation. Even so, the simulation results in Fig. 11 show that both controllers achieve their respective goals of phase difference and apex height.

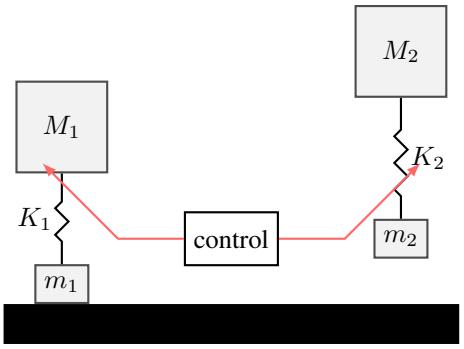

Fig. 10: The hybrid system of two coupled bouncing masses.

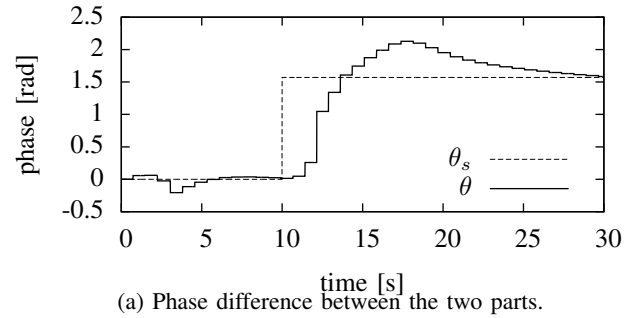

(a) Phase difference between the two parts.

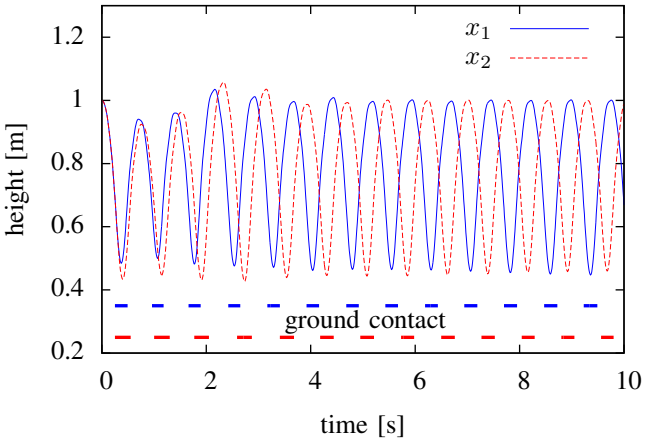

(b) Mass height (top) and ground contact (bottom).

Fig. 11: Simulation results for the two-part hopping robot.

V. Conclusions

In this paper, we have demonstrated an intuitive way to achieve phase synchronisation in oscillating physical systems. Moreover, it is a power-continuous method: the control signal only modulates a gyration ratio, so that the overall system is completely passive.

The drawback of this method, the fact that the energy exchange between the oscillators changes their amplitudes, has been addressed by a separate energy level controller that is in itself also power-continuous, modulating the power flow between the oscillators and a buffer. Only when increasing the power level of both oscillators combined do we actually need to use the energy from the buffer itself.

In the analysis, we have mainly considered ideal components that have no losses and allow for infinitely rapidly changing gyration and modulation ratios, so the question arises whether the method also works for real-world applications. The simulation experiment with bouncing masses showed that the strategy indeed manages synchronisation in a more realistic situation. However, by using a regular variable stiffness actuator the system is unfortunately no longer power-continuous. To solve this problem we are investigating mechanisms that can physically connect the two springs and achieve synchronisation in an energy-free way.

We hope that these power-based control strategies, which fit well into a morphological computation framework, will help us and other researchers in developing truly high-speed, energy-efficient locomotion.

References

[1] J. Svensson, "Synchronisation methods for grid-connected voltage source converters," *Generation, Transmission and Distribution, IEE Proceedings-*, vol. 148, no. 3, pp. 229–235, 2001.

[2] A. J. Ijspeert, "Central pattern generators for locomotion control in animals and robots: A review," *Neural Networks*, vol. 21, no. 4, pp. 642 – 653, 2008, ¡ce:title¿Robotics and Neuroscience¡/ce:title¿. [Online]. Available: http://www.sciencedirect.com/science/article/pii/S0893608008000804

[3] A. Crespi and A. J. Ijspeert, "Amphibot ii: An amphibious snake robot that crawls and swims using a central pattern generator," in *Proceedings of the 9th international conference on climbing and walking robots (CLAWAR 2006)*, vol. 11, no. 7-8. Citeseer, 2006, pp. 19–27.

[4] J. Conradt and P. Varshavskaya, "Distributed central pattern generator control for a serpentine robot," in *Proceedings of the International Conference on Artificial Neural Networks (ICANN)*, 2003, pp. 338–341.

[5] N. Maheshwari, X. Yu, M. Reis, and F. Iida, "Resonance based multi-gaited robot locomotion," *2012 IEEE/RSJ International Conference on Intelligent Robots and Systems*, pp. 169–174, Oct. 2012. [Online]. Available: http://ieeexplore.ieee.org/lpdocs/epic03/wrapper.htm?arnumber=6385618

[6] R. Pfeifer and F. Iida, "Morphological computation: Connecting body, brain and environment," *Japanese Scientific Monthly*, vol. 58, pp. 48–54, 2005. [Online]. Available: http://people.csail.mit.edu/iida/papers/pfeifer_iida_JSM05.pdf

[7] J. Acebrón, L. Bonilla, and C. Vicente, "The Kuramoto model: A simple paradigm for synchronization phenomena," *Reviews of Modern Physics*, vol. 77, no. January, 2005. [Online]. Available: http://rmp.aps.org/abstract/RMP/v77/i1/p137_1

[8] S. H. Strogatz, "From Kuramoto to Crawford: exploring the onset of synchronization in populations of coupled oscillators," *Physica D: Nonlinear Phenomena*, vol. 143, no. 1-4, pp. 1–20, Sep. 2000. [Online]. Available: http://linkinghub.elsevier.com/retrieve/pii/S0167278900000944

[9] W. Ren, "Synchronization of coupled harmonic oscillators with local interaction," *Automatica*, vol. 44, no. 12, pp. 3195–3200, Dec. 2008. [Online]. Available: http://linkinghub.elsevier.com/retrieve/pii/S0005109808003580

[10] P. Perlikowski, A. Stefaski, and T. Kapitaniak, "1:1 Mode locking and generalized synchronization in mechanical oscillators," *Journal of Sound and Vibration*, vol. 318, no. 1-2, pp. 329–340, Nov. 2008. [Online]. Available: http://linkinghub.elsevier.com/retrieve/pii/S0022460X08003738

[11] J. Buchli, F. Iida, and A. Ijspeert, "Finding Resonance: Adaptive Frequency Oscillators for Dynamic Legged Locomotion," in *2006 IEEE/RSJ International Conference on Intelligent Robots and Systems*. Ieee, Oct. 2006, pp. 3903–3909. [Online]. Available: http://ieeexplore.ieee.org/lpdocs/epic03/wrapper.htm?arnumber=4059016

[12] A. van der Schaft, "Port-Hamiltonian systems: an introductory survey," in *Proceedings of the International Congress of Mathematicians*, vol. III, Madrid, Spain, 2006, pp. 1339–1365, invited Lectures, eds. Marta Sanz-Sole, Javier Soria, Juan Luis Verona, Joan Verdura.

[13] Controllab Products B.V., "20-sim," http://www.20sim.com/, 2013.